ACS Catalysis

pubs.acs.org/acscatalysis Research Article

Mechanistic Investigation of a Photocatalyst Model Reveals Function by Perylene-Like Closed Shell Super-Photoreductant Capable of Reducing Unactivated Arenes

Arindam Sau,[▽] Nicholas F. Pompetti,[▽] Alexander R. Green,[▽] Mihai V. Popescu, Robert S. Paton, Garret M. Miyake,* and Niels H. Damrauer*

Cite This: *ACS Catal.* 2024, 14, 2252−2263 Read Online

ACCESS | Metrics & More | Article Recommendations | Supporting Information

ABSTRACT: Benzo[*ghi*]perylene monoimides (BPIs) have recently been employed as organic photocatalysts for challenging reductions. In probing their function, we identify a thermal degradation product involving imide ring opening, and this in turn motivates the development and synthesis of a high-symmetry model system—a benzo[*ghi*]perylene diester (**BPDE**)—whose structural simplicity is useful for mechanistic exploration relevant to the broader photocatalyst class. Using electrochemical and spectroscopic tools, we probe both the singly and doubly reduced states of **BPDE** and report the generation of [**BP-H**]$^-$, a two-electron, one-proton activated closed-shell super-reductant. This catalytically active species, after visible photon absorption, operates from its singlet excited state, where the motions of the added proton are coupled to an electron transfer event, which enables direct reduction of inert substrates like benzene and fluorobenzene. Traditional Birch chemistry on benzene has been previously realized only by solvated electrons or electrochemistry. The function of this model system uncovered in these mechanistic explorations suggests modes of operation for this photocatalyst class that will enable future optimizations.

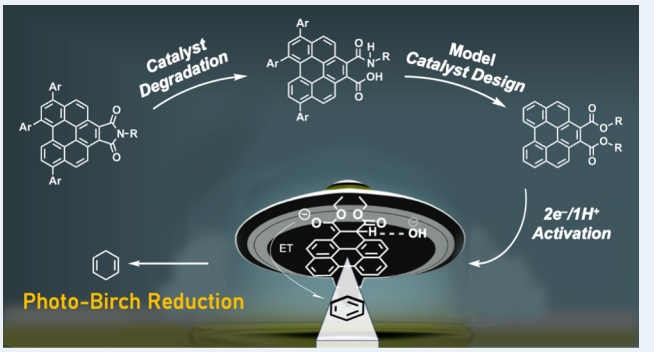

KEYWORDS: *Birch reduction, photoredox catalysis, quenching, super reductant, excited-state redox, aryl−fluoride bond activation, defluorination, proton-coupled electron transfer*

INTRODUCTION

Using visible light to activate small molecules through redox processes is a growing strategy for synthetic chemists.[1−6] For processes driven by the absorption of a single photon in a photocatalyst (PC), an absolute potential of >3 V is in principle achievable considering that 400 nm photons in the blue edge of the visible spectrum carry 3.1 eV of energy. However, additional electrochemical and photochemical considerations significantly limit what potentials can be deployed. For example, from the perspective of PCs that drive reductive transformations, one must also consider the PC oxidation potential as well as loss of energy prior to a successful electron transfer to a target substrate due to nonradiative intra-PC phenomena. In practice, reductive transformations requiring more than ca. −2 V cannot be carried out without harvesting the combined energies of more than one photon. Following the work of Ghosh et al., where aryl halides including aryl chlorides could be activated using perylene diimide (PDI) and 440 nm blue light,[7] several organic and metal-based photocatalytic systems have been developed that rely on consecutive photoinduced electron transfer events (ConPET).[8] In such systems, an initial photoinduced redox event modifies the PC, which then absorbs a second photon to produce a highly redox-potent excited state. This general scheme has been invoked in describing the function of highly reducing organic photocatalytic dyes,[9,10] with implantation in synthetic transformations such as dehalogenations,[7,11,12] detosylations,[13] and Birch reductions.[14,15]

Several of the organic photosensitizers developed to utilize ConPET (xanthones,[16] dicyanoanthracenes,[17] and napthalene and perylene imides[18]) are proposed to operate out of an open-shell PC intermediate that allows for a single electron transfer (SET) from the excited doublet to the substrate. However, PCs that operate from an open-shell state are air-sensitive and often demonstrate short excited-state life-

Received: November 8, 2023
Revised: December 17, 2023
Accepted: December 20, 2023
Published: January 29, 2024

https://doi.org/10.1021/acscatal.3c05386
ACS Catal. 2024, 14, 2252−2263

times[10,18,19] that can limit diffusional bimolecular electron transfer yields, thereby impacting their synthetic utility.[10] On the other hand, the open-shell radical anionic states of the PCs can in principle be further reduced to generate closed-shell species (for example, of polyaromatic imide photocatalysts[20,21]) that are more stable with much longer excited-state lifetimes. These may also be able to act as potent photoreductants. For example, as illustrated by Rieth et al., the doublet excited state of naphthalene monoimide radical anion ($NMI^{\bullet-}$) only lives for 24 ps, whereas the closed-shell Meisenheimer-like $[NMI(H)]^-$ complex that is electrochemically produced and represents the further addition of an electron and a proton shows a ∼3 orders of magnitude longer fluorescence lifetime of 20 ns while at the same time having a comparable excited-state reduction potential (≈ −3.1 V vs Fc^+/Fc).[20] Importantly, $[NMI(H)]^-$ was shown to act as a reductant with methyl-4-chlorobenzoate under 440 nm irradiation. The reactivity of this system suggests that a closed-shell reductant is operative.

Discovered by Cole et al. in 2020, the benzo[*ghi*]perylene imide (BPI) photocatalyst family exhibits potency for the Birch reduction of unactivated arenes,[14] which traditionally requires the use of pyrophoric metals (Na and Li) and liquid ammonia.[22,23] However, long reaction times and the need for multiple catalyst loadings limit the practical application of the photo-Birch system in synthesis (Figure 1A). Rational catalyst

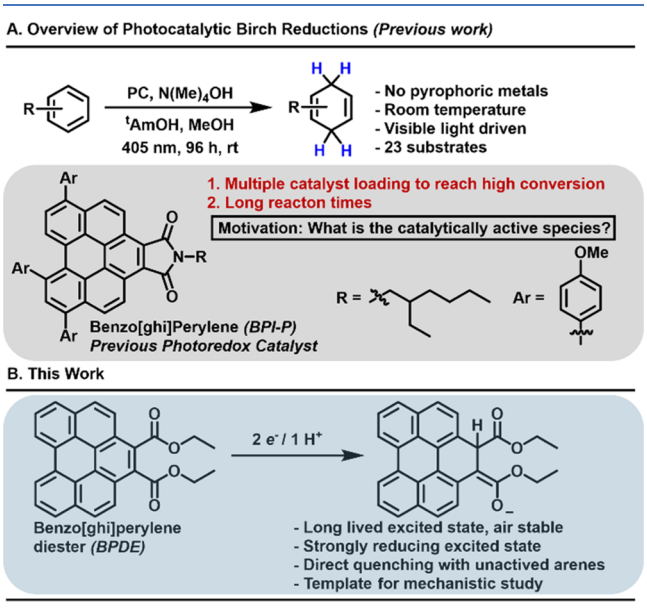

Figure 1. (A) Previous scheme for visible-light-driven Birch reduction using BPI photocatalysts and their identified limitations. (B) Activation pathway using newly developed **BPDE**.

design with improved reactivity would require a priori knowledge of major photodegradation pathways, along with mechanistic understanding of the photoactive redox state of the PC, as demonstrated in PDI and cyano-arene-based organic PCs.[24,25] In this current work, we show that the major degradation of BPI catalysts involves the hydrolysis of the imide ring, motivating the synthesis of a new PC (benzo[*ghi*]-perylene diester or **BPDE**) that bypasses imide hydrolysis and provides a structurally simpler platform through its symmetry for spectroscopic interrogation. Through the use of cyclic voltammetry, spectroelectrochemistry, absorption spectroscopy, and fluorimetry, we probe both the singly and doubly reduced states of **BPDE** and identify the relevant highly reducing photoactive redox state. Although the yield of photo-Birch via **BPDE** is low, its use as a model for this mechanistic exploration uncovers a critical mode of operation for this class of photocatalysts that will enable future optimizations.

RESULTS AND DISCUSSION

Challenges Emerge Improving Original PC Design Even after Introducing Enhanced Solubility. As noted above, major limitations for the practical application of BPI derivatives in photo-Birch stem from long reaction times and requirements for multiple catalyst loadings.[14] We initially hypothesized that long reaction times were due to the poor solubility of **BPI-P** (structure in Figure 2A) in methanol, resulting in a predominately heterogeneous system. Since benzyl alcohol substituents are known to solubilize metalloporphyrin complexes in water or alcoholic solvent,[26] a derivative was synthesized using 4-benzyl alcohol as the core extension substituent (**BPI-M**, Figure 2A), and this PC proved to be methanol-soluble. Notably, the thermodynamic and photophysical properties are not significantly perturbed (Table S5, Figure S15). Using the same reaction conditions as those previously reported, the conversion of benzene to cyclohexadiene was monitored to benchmark performance. However, even with a completely homogeneous system, this PC did not show a better performance. In 48 h, **BPI-M** drives 30% conversion of benzene to cyclohexadiene, 5% lower than what was observed using **BPI-P** (Table S2).

Observations of Underlying Hydroxide-Induced Structural Changes to BPI. Although the overall photo-Birch reaction time and yield were not improved, the enhanced solubility of **BPI-M** enabled in situ spectroscopic monitoring under relevant reaction conditions. First, we probed the interaction of BPI-M with tetramethylammonium hydroxide (TMAOH) under the hypothesis that hydroxide could lead to the degradation of the catalyst. Upon addition of TMAOH to a solution of **BPI-M** in methanol, the charge transfer (CT) transition[27] centered at 500 nm in the UV−vis spectrum is lost with a concomitant appearance of a new band centered at 408 nm (Figure 2C). The observed change demonstrates a thermal reaction with OH^- resulting in a new species, denoted $[\mathbf{BPI\text{-}M{-}OH}]^-$. This solution was then irradiated with 405 nm light, wherein the broad 408 nm absorption band was rapidly lost and a spectrum emerged that was characterized by two well-resolved features centered at 374 and 392 nm (Figure 2C). Notably, this change persists, and we do not observe the reformation of $[\mathbf{BPI\text{-}M{-}OH}]^-$ or **BPI-M** after monitoring the solution for 24 h, suggesting that the catalyst has undergone a light-driven structural change.

Parallel to the UV−vis absorption measurements, the associated structural changes of **BPI-M** with TMAOH were tracked in situ using ^{13}C NMR and high-resolution mass spectrometry (HRMS). The ^{13}C NMR spectrum collected for **BPI-M** shows a single resonance at 170 ppm assigned to the imide carbonyl carbon and indicates that core-substitutional asymmetry in this molecule is sufficiently remote from this site to obviate detection of two different ^{13}C resonances. Analysis of the product associated with $[\mathbf{BPI\text{-}M{-}OH}]^-$, on the other hand, reveals the emergence of a new signal at 176 ppm. The significance of this resonance within a region associated with carbonyl ^{13}C sites argues against an intact imide ring after nucleophilic addition of OH^-, since this would result in the

https://doi.org/10.1021/acscatal.3c05386
ACS Catal. 2024, 14, 2252−2263

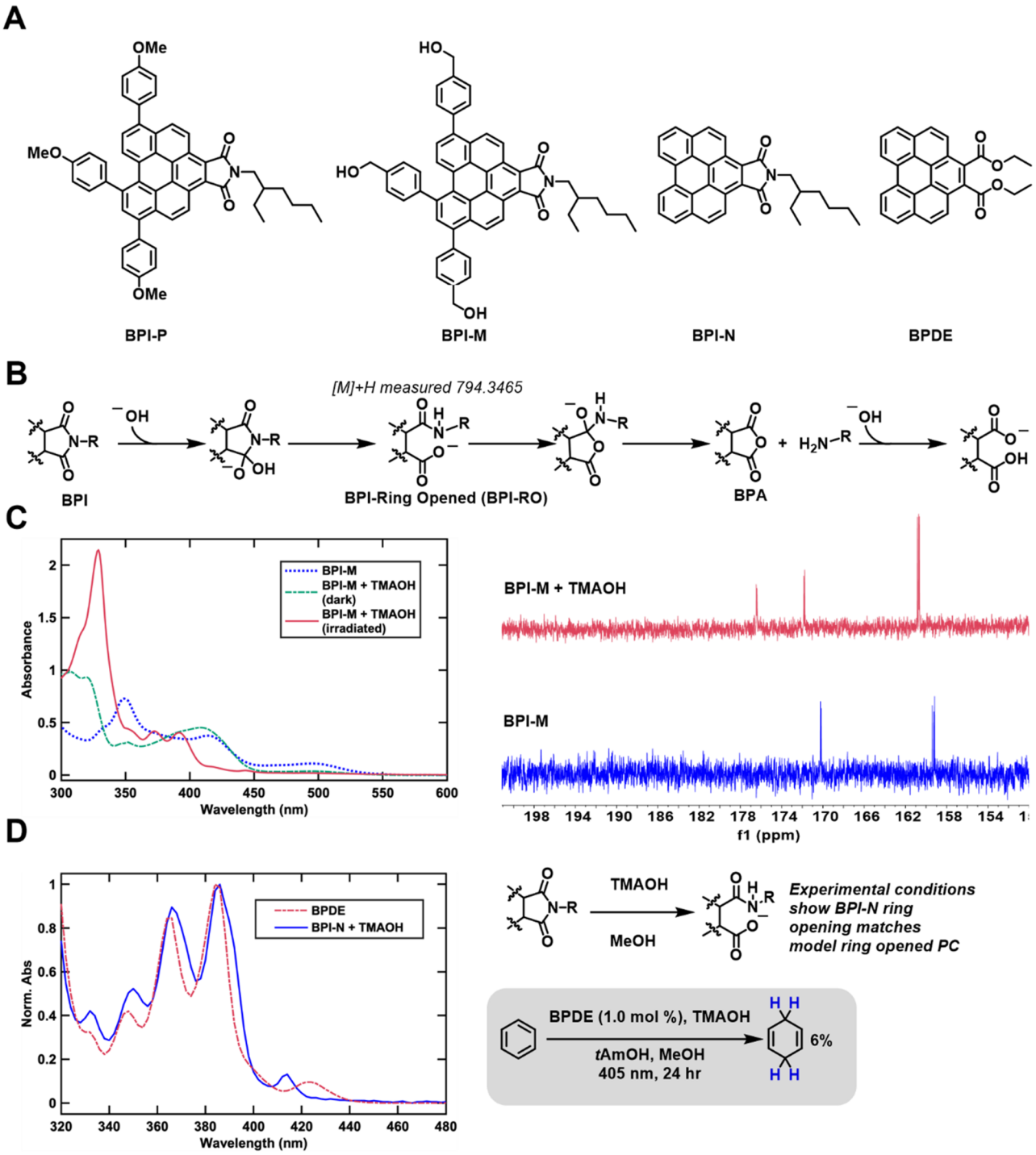

Figure 2. (A) Photocatalysts used in mechanistic study. (B) Proposed mechanism for the thermal degradation of **BPI-M** via hydroxide. (C) Absorbance and ^{13}C NMR spectra monitoring the changes associated with **BPI-M** interacting with TMAOH in methanol. (D) Absorbance spectra highlighting the similarities between the newly synthesized **BPDE** and **BPI-N** in the presence of TMAOH. **BPDE** can act as a model ring-opened catalyst comparable to the thermally ring-opened **BPI-N** structure.

formation of an sp^3-hybridized carbon center (Figure 2B). Instead, this signal suggests a chemical inequivalence for a pair of carbonyl sites. We posit that this chemical inequivalence is due to imide ring-opening in the presence of OH^-, resulting in carboxylate and amide functionalities. Imide hydrolysis in the presence of OH^- has been previously reported.[28] Additionally, it is noted that breaking of the imide ring would explain the loss of the lowest-energy CT band. An aliquot of the crude mixture (**BPI-M** + TMAOH) was analyzed using HRMS, and a signal was observed that matched the predicted mass of the protonated ring-opened species: BPI-Ring Opened (**BPI-RO**) (Figure 2B). We attempted to isolate **BPI-RO** to explore whether it is active on its own in photo-Birch. However, this compound proved to be sensitive to ring-closure during isolation of this transient species. In reaction conditions we found that through an acid workup (with slowly added 0.1 M HCl), the crude mixture containing **BPI-RO** is driven to a benzo[*ghi*]perylene anhydride (**BPA**, Figure 2B). The **BPA**

https://doi.org/10.1021/acscatal.3c05386
ACS Catal. 2024, 14, 2252−2263

compound exhibits some properties akin to those of **BPI-M**, including a CT-like transition and a single carbonyl signature (164 ppm in $CDCl_3$) in the ^{13}C NMR spectrum. As a photocatalyst, however, **BPA** is less effective than the parent (20% conversion of benzene to cyclohexadiene monitored via ^1H NMR in 24 h as compared to 30% using **BPI-M**).

Motivation for a Ring-Opened Model System. Due to the poorer reactivity of **BPA** in the photo-Birch reduction of benzene, we hypothesized that **BPI-RO** is relevant to reactivity. However, because **BPI-RO** is challenging to isolate, a model photocatalyst was sought that was representative of the ring-opened species but stable against anhydride formation. Recognizing that a benzo[*ghi*]perylene diester would represent one of the simplest proxies for **BPI-RO**, we synthesized **BPDE** (Figure 2A) using a one-pot Diels–Alder cycloaddition between perylene and diethyl acetylenedicarboxylate. Notably, the UV–vis absorption spectrum is similar to that seen for the non-core-extended **BPI-N** (Figure 2A) after exposure to hydroxide (Figure 2D). Spectral features of **BPDE** are highlighted by the relatively weak α-band (Clar's notation[29]) at ∼425 nm, which acts as the lowest electronic excited state (S_1), whereas the more prominent p-band (S_2) is vibronically resolved with the 0–0 transition centered at 385 nm. The new **BPDE** functions as a photocatalyst in the reduction of benzene to cyclohexadiene (6% conversion). This efficacy is comparable to that of **BPI-N**, which exhibits 3% conversion as reported previously.[14] **BPDE** also exhibits reactivity in the hydrodehalogenation of fluorobenzene and chlorobenzene, in which benzene formation was monitored via NMR, albeit in low NMR yields (19% on fluorobenzene, 25% on chlorobenzene) (Figure S1). We note that in terms of performance, **BPDE** is inferior to the higher performing **BPI-P**. However, the observed photoinduced substrate reduction reactivity suggests that **BPDE** can indeed be used as a model ring-opened compound for further mechanistic understanding and can act as a template for future modification. Understanding how the aryl substitutions onto the benzo[*ghi*]perylene core affect PC performance is currently being studied.

Photochemical Investigation of BPDE Reveals a New Species Whose Fluorescence Is Quenched by Benzene. The general function as a photocatalyst in both Birch and hydrodehalogenation, combined with the simplicity and symmetry of the compound, motivated us to explore how this model PC functions during photocatalysis. We began by monitoring **BPDE** reactivity with excess TMAOH (∼5000 equiv) in the dark via UV–visible spectroscopy in a THF/MeOH (2:1) solvent system. THF was used as a cosolvent because **BPDE** is insoluble in pure MeOH. As shown in Figure S20A, the absorption spectrum of **BPDE** remains the same upon the introduction of OH^- other than the expected dilution effect due to the added MeOH. Next, we sought to explore if photoexcited **BPDE** would react with TMAOH. This reaction was performed by irradiating **BPDE** in the presence of 180 mM TMAOH (∼5000 equiv) inside a photoreactor fitted with two 385 nm LEDs. As shown in Figure 3A, the vibronic absorption peaks of the parent benzo[*ghi*]perylene core diminish over minutes, concomitant with the appearance of two new peaks at 425 and 445 nm that resemble a new red-shifted vibronic progression. Observation of an isosbestic point at 390 nm suggests a 1-to-1 conversion from **BPDE** to another species. During this absorption spectrum sequence, photoluminescence spectra were also collected after each period of irradiation. As can be seen in Figure 3B, a bright vibronically

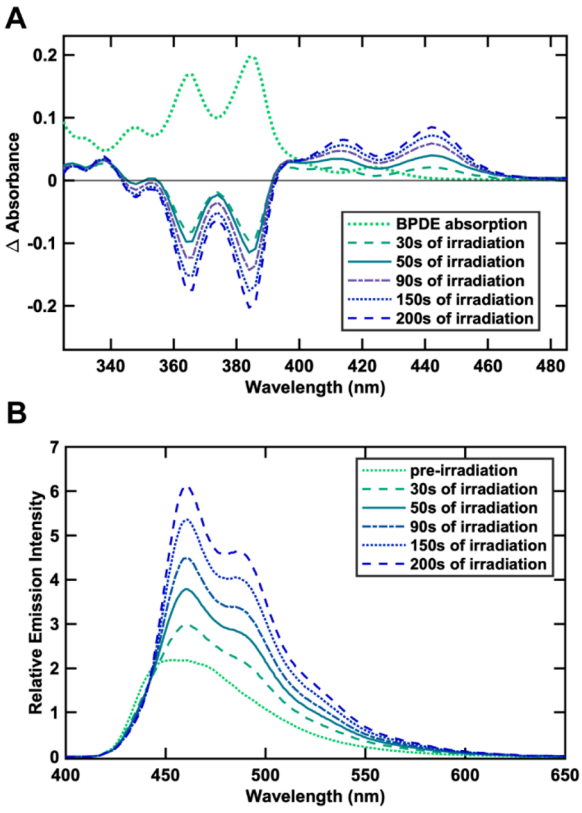

Figure 3. Changes in the (A) absorption and (B) emission spectra of 35 μM **BPDE** under irradiation in the presence of 180 mM TMAOH in a 2:1 THF/MeOH solvent system. The emission spectra were collected by exciting the sample at 420 nm.

resolved spectrum emerges that is distinct from the broad and featureless fluorescence spectrum of **BPDE**. A quantum yield determination after 200 s of irradiation indicates Φ_{em} = 0.94 for the new species (Figure S23). It also has a fluorescence lifetime of ∼7 ns, which is shorter compared to that of **BPDE** (τ_{em} = 16.2 ns). At the same time, the newly formed species was found to be tolerant to air exposure even after 24 h, which, along with a very high emission quantum yield and multinanoseconds lifetime, suggests that it is not an open-shelled radical anion. In a preliminary consideration of the role played by this new species within catalysis, photoluminescence spectra were recorded in the presence of substrate. Selective photoexcitation for the new species at 450 nm was required because these samples still maintained unreacted **BPDE**. Interestingly, the fluorescence intensity of the new species is found to be diminished after the addition of benzene (Figure S24). For example, in the presence of 0.30 M benzene, the 0–0 peak height decreased by 11%. This is, to our knowledge, evidence for the first example of the excited-state reactivity of an organic photoreductant observed in the presence of an arene as inert as benzene. More detailed explorations of quenching properties are explored later in this work after identification of the emitting chromophore and establishment of protocols to more cleanly produce it for more systematic explorations.

Electrochemical and Spectroelectrochemical Interrogation of BPDE: Connecting Redox Events to Photochemical Product. Cole et al. previously demonstrated that OH^- was critical for **BPI-P**-driven photo-Birch reactivity. To understand the role of hydroxide in our system as an electron

https://doi.org/10.1021/acscatal.3c05386
ACS Catal. 2024, 14, 2252–2263

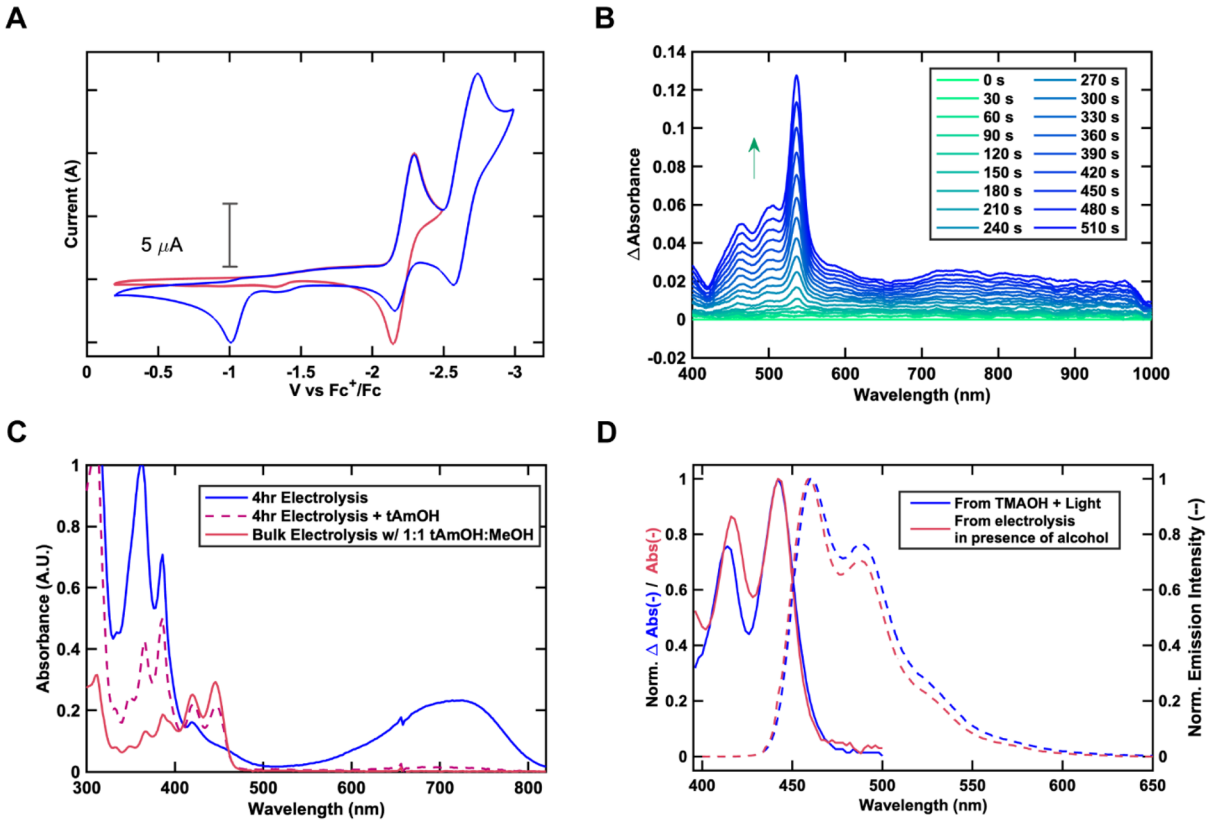

Figure 4. (A) Cyclic voltammograms of 1.0 mM **BPDE** in 0.1 M $TBAPF_6$ THF solution, scanning at 100 mV s^{-1} from 0 to −2.5 V (pink trace) and from 0 to −3.0 V (blue trace) vs Fc^+/Fc using a Pt disk working electrode, Pt wire counter electrode, and leak-free $Ag/AgNO_3$ reference electrode. (B) Spectroelectrochemical study of **BPDE** in 0.1 M $TBAPF_6$ THF solution with the Pt mesh working electrode held just past the $1e^-$ reducing potential at −2.4 V vs Fc^+/Fc. (C) Absorbance spectra of **BPDE** after 4 h of bulk electrolysis at −2.85 V vs Fc^+/Fc in THF (blue), the bulk electrolyzed solution following the addition of tAmOH (dashed pink), and the solution after continued bulk electrolysis at −2.85 V vs Fc^+/Fc in a 2:0.5:0.5 THF/MeOH/tAmOH solvent system (red). (D) Comparison of the absorption and emission spectra of the electrochemically formed $[\mathbf{BP\text{-}H}]^-$ species to that formed by the reaction of **BPDE**, irradiation at 405 nm for 200 s, and TMAOH.

donor, we were motivated by the work reported by Saha et al., who showed that electron rich anions are capable of reducing π-acids in their ground state or upon photoexcitation.[30,31] In order to investigate the reduced states of **BPDE**, we turned to electrochemistry, replacing the chemical reductant with an electrode. Cyclic voltammetry studies of **BPDE** are shown in Figure 4A. In experiments that sweep with a negative potential limit of −2.5 V vs Fc^+/Fc, a first redox event occurs in THF that is reversible with a half-wave potential of −2.22 V vs Fc^+/Fc. This potential corresponds to $\mathbf{BPDE} + e^- \rightleftharpoons \mathbf{BPDE}^{\bullet-}$. When scanning into more negative potentials, a second redox event is observed with a half-wave potential of −2.61 V vs Fc^+/Fc that corresponds to the dianion formation $\mathbf{BPDE}^{\bullet-} + e^- \rightleftharpoons \mathbf{BPDE}^{2-}$. However, this redox event displays an apparent diminished return current (anodic peak) of the first reduction (see Figure 4A), and likely second reduction, and is accompanied by the appearance of a new anodic-current feature seen at approximately −1.00 V vs Fc^+/Fc. These observations together suggest that a chemical product formed at negative potentials capable of dianion formation (more negative than −2.62 V vs Fc^+/Fc), then requires a substantively positive potential (more positive than ∼ − 1 V vs Fc^+/Fc) to return **BPDE**. The reversibility of this wave exhibits scan-rate dependence: after the scan rate increases from 0.1 to 0.4 V/s, the new feature exhibits partial reversibility (cathodic current) and an approximate $E_{1/2}$ = −1.1 V vs Fc^+/Fc (Figure S10).

Spectral characterization of the one-electron reduction product $\mathbf{BPDE}^{\bullet-}$ via spectroelectrochemistry is presented in Figure 4B. In THF, a progression of peaks is observed at 463, 504, and 537 nm, as well as a broad and featureless absorption extending well past the 1000 nm detection limit of the spectrometer. The intense peak at 537 nm is consistent with the reported absorption spectrum of the benzo[*ghi*]perylene radical anion.[32] Notably, these features do not match with the emergent vibronic progression observed for **BPDE** under irradiation in the presence of TMAOH (Figure 3A). We attempted to generate $\mathbf{BPDE}^{\bullet-}$ within THF via bulk electrolysis in order to analyze its excited-state lifetime by transient absorption. However, after removal of the electrode, the radical anion was unstable even under a strictly inert atmosphere and without any substrate present, as observed through UV−vis changes on a minute time scale, and this made transient absorption characterization difficult. As a surrogate, bulk electrolysis was performed to generate the radical anion of the parent catalyst, i.e., $\mathbf{BPI\text{-}P}^{\bullet-}$, which was more stable (generated in DMAc at −2 V vs Fc^+/Fc). TA experiments indicate that $\mathbf{BPI\text{-}P}^{\bullet-}$ has a lifetime of ∼10 ps. (Figure S18). Such a short-lived excited state is expected to preclude the radical anion from engaging in excited-state reactivity via diffusion-limited bimolecular collisions. From these observations, and the UV−vis absorption dissimilarity with irradiated **BPDE** in the presence of TMAOH (Figure 3A), it is unlikely that the radical anion is operative in the

https://doi.org/10.1021/acscatal.3c05386
ACS Catal. 2024, 14, 2252−2263

reduction of substrates as a major pathway in the photo-Birch mechanism. Similar challenges in directly using an organic radical anion to drive photoinduced electron transfer reactions with solution phase substrates have recently been noted by others as well in their consideration of both monoimide[20] and diimide[21] species. Hence, we move our investigation to doubly reduced **BPDE**$^{2-}$ and its relationship to the new oxidative feature found in cyclic voltammetry.

Spectral characterization after the second reductive wave using spectroelectrochemistry encounters some complexity due to kinetic considerations involving the sequential conversion of species during the measurement. Only after the majority of the starting material **BPDE** was converted to the radical anion would a doubly reduced product start to form. Given the small Pt mesh used for the spectroelectrochemical experiments, conversion of **BPDE**$^{\bullet-}$ to **BPDE**$^{2-}$ is slow. As such, we engaged in longer bulk electrolysis experiments to drive more product formation in an H-cell using a larger glassy carbon working electrode. A sequence of three related experiments is shown in Figure 4C. *First*, a concentrated solution of **BPDE** in THF (with 0.1 M $TBAPF_6$) was electrolyzed at −2.85 V vs Fc^+/Fc for 4 h. The UV−vis absorption spectrum of an aliquot taken from the H-cell is shown in the blue trace and indicates the emergence of new absorption features, including a broad band at ∼710 nm and an intense peak at 360 nm, which are assigned to **BPDE**$^{2-}$. We suspect that the sharp shoulder at 386 nm is due to **BPDE** suggesting that bulk electrolysis is not complete. However, there is no evidence of **BPDE**$^{\bullet-}$ given the absence of a peak at 537 nm. *Second*, we then considered spectral changes upon addition of an alcohol to the aliquot taken from the H-cell, guided by the fact that the reaction conditions rely on inclusion of *tert*-amyl alcohol (tAmOH) or MeOH environments. As can be seen in the dashed purple trace of Figure 4C, addition of 200 μL of tAmOH (see Figure S12 for a similar experiment using MeOH) leads to the loss of the prominent ∼710 and 360 nm features. A vibronic progression peak at 386 nm becomes evident as the 360 nm band is lost, and this corresponds to the starting **BPDE** that had not been electrolyzed (vide supra). Importantly, we also observe the emergence of a pair of peaks at 420 and 446 nm suggestive of a second vibronic progression. These are effectively coincident with the peaks observed when **BPDE** is irradiated in the presence of TMAOH in a THF/MeOH mixture (Figure 3A). *Third*, returning to the H-cell, 1.00 mL of 1:1 tAmOH/MeOH was added, and electrolysis was continued for 1 h at −2.85 V vs Fc^+/Fc. As shown in the red trace of Figure 4C, the system appears to drive closer to completion of the product, characterized by the vibronic progression peaking at 446 nm. A small amount of **BPDE** remains evident, as inferred, for example, by the structured peak shape of the 0−2 vibronic transition. The absorption spectrum from this experiment is shown in Figure 4D superposed with the difference absorption data from Figure 3A after **BPDE** was irradiated for 200 s in the presence of TMAOH in a THF/MeOH mixture. The spectral similarity highlights that the same product is emerging in both electrochemical and photolysis experiments, supporting the idea that hydroxide can act as a sacrificial electron donor to **BPDE**. Figure 4D also shows a close correspondence between emission spectra collected following excitation at 450 nm for both samples.

Two-Electron, One-Proton Activation of BPDE Forms a Catalytically Active Species [BP-H]$^-$. Taken as a whole, the electrochemical observations suggest that in THF, in the absence of a proton source, the primary electrolysis product (−2.85 V vs Fc^+/Fc) is **BPDE**$^{2-}$. When protons are available (e.g., tAmOH or MeOH), either upon addition of a protic solvent to a mixture of **BPDE**$^{2-}$ and **BPDE** (second experiment above) or during active electrolysis that is producing **BPDE**$^{2-}$ from **BPDE** in the presence of a protic solvent (third experiment above), a stable product is formed whose absorption spectral features match the photochemical product generated when **BPDE** is irradiated in the presence of TMAOH in a THF/MeOH mixture (Figure 3A). Without TMAOH, **BPDE** upon irradiation shows no changes, as monitored by UV−vis, suggesting that TMAOH is needed to generate [**BP-H**]$^-$ (Figure S20B). To understand the CV data of Figure 4A in this context, we posit that at large negative potentials— beyond the $E_{1/2}$ = −2.61 V vs Fc^+/Fc needed to generate **BPDE**$^{2-}$—the same product is formed with an amount limited by the availability of protons and the scan rate competing with the rate of product formation. Although the CV experiment was run in THF, some proton availability is possible through the presence of tetrabutylammonium, a source of protons through Hofmann elimination.[33] Addition of tAmOH, a protic solvent, to the CV solution reduces the reversibility of the first and second wave in further support of our hypothesis (see Figure S11 for details). Since the new species is formed in the presence of protons following the generation of the **BPDE**$^{2-}$, we hypothesize that the catalytically active species under photo-Birch conditions is a two-electron, one-proton activated closed-shell reductant [**BP-H**]$^-$. Similar hydride complexes can be seen in a napthalene monoimide species that was recently reported by Rieth et al.[20]

The anodic current wave that emerges at −1.00 V vs Fc^+/Fc thus appears to involve the oxidation of [**BP-H**]$^-$. To explore this further, changes to the electrochemically generated [**BP-H**]$^-$ were monitored via spectroelectrochemistry in THF after shifting the transparent working electrode potential to −0.4 V vs Fc^+/Fc. As seen in Figure 5, the vibronic features associated with [**BP-H**]$^-$ (420 and 450 nm) decrease in intensity, while features associated with ground-state **BPDE** reappear. There is no spectral evidence of any other intermediates within the 300−1000 nm spectral window during the conversion. This

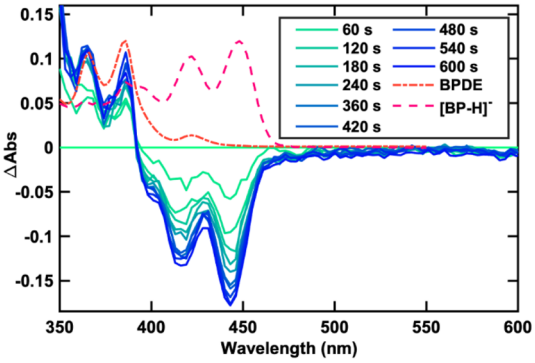

Figure 5. Spectroelectrochemistry of [**BP-H**]$^-$, shown as ΔAbs, highlighting spectral changes in the vibronic progression when held at a potential at −0.4 V vs Fc^+/Fc. The applied potential oxidizes [**BP-H**]$^-$ as seen from the gradual decrease in the 420−450 nm vibronic progression. However, a simultaneous growth of a blue-shifted vibronic progression that matches the absorption of **BPDE** indicated that upon oxidation [**BP-H**]$^-$ undergoes structural changes to reform benzoperylene. The ground-state **BPDE** and [**BP-H**]$^-$ absorbance spectra are included for comparison.

https://doi.org/10.1021/acscatal.3c05386
ACS Catal. 2024, 14, 2252−2263

observation leads us to the conclusion that at potentials appropriate for oxidation, [**BP-H**]$^-$ undergoes structural rearrangements needed to rearomatize back to **BPDE**. The observation is consistent with one-electron oxidation of [**BP-H**]$^-$ followed by the spontaneous loss of a second electron and a proton at this potential. This in turn is consistent with the expected ∼2 V driving force for the oxidation of **BPDE**$^{\bullet-}$ given that the **BPDE**/**BPDE**$^{\bullet-}$ couple is at −2.22 V vs Fc^+/Fc V (Figure 4A). A similar observation using electrochemistry was made in the case of [NMI(H)]$^-$ as well.[20]

Computational and Spectral Indications for the Formation of Perylene-Like [BP-H]$^-$. We turn to the question of the likely structure of [**BP-H**]$^-$, envisioning the gain of two electrons and one proton as effectively a hydride transfer to **BPDE** in order to propose a possible set of isomers. These structures are shown in Figure S52, although a single chromophore is expected on the basis of the single photoluminescence decay constant (∼7 ns) observed for [**BP-H**]$^-$ in both the electrolysis (Figure S26) and photolysis experiments (Figure S22) in the presence of a proton source (vide supra). Our intuition at the outset was that a perylene-like structure (isomer *AA* in Figure S52) was most likely to form, generated from a dianion where the negative charges lie toward the ester head, followed by protonation then tautomerization (see a scheme of anticipated events in Figure S14). An extensive thermochemical computational exploration that is also summarized within Figure S52 (see the SI for further details) supports a perylene structure with the energy of *AA* being the lowest of these isomers by a substantial amount in most cases and 7.8 kcal/mol for the closest isomer (*G*), which is represented by hydride transfer to a benzoperylene bay position. Furthermore, our calculations reveal a one-electron redox potential of −1.27 ± 0.29 V vs Fc^+/Fc for the *AA* isomer (Figure S50). This value aligns well with the partially reversible wave at −1.10 V Fc^+/Fc for the cathodic current observed in the CV measurements (Figure S10). It is noted that the polyaromatic hydrocarbon (PAH) core of isomer *AA* resembles perylene (Pe), to be contrasted with other PAH forms, including benzo[*e*]pyrene, pyrene, phenanthrene, oxidized olympicene, and others. All photophysical data that we have collected are in support of a closed-shell Pe-like species. For example, the absorption spectrum of [**BP-H**]$^-$ is red-shifted into the visible region with the 0−0 peak of the vibronic progression at 442 nm, only 8 nm relative to pure Pe in EtOH, where the peak is at 434 nm (Figure S25). The emission spectrum of [**BP-H**]$^-$ is also similar to Pe, although the Stokes shift for [**BP-H**]$^-$ at 17 nm is larger than that for its PAH parent (4 nm, Figure S25), suggesting more reorganization within the [**BP-H**]$^-$ singlet excited state prior to emission, perhaps as a result of inclusion of partial charge-transfer character involving the enolate substituent. The high emission quantum yield of [**BP-H**]$^-$ is consistent with Pe. Finally, we were able to investigate the transient absorption characteristics of [**BP-H**]$^-$. As shown in Figure 6, it exhibits an intense excited-state absorption at ∼700 nm with a bluer shoulder at 635 nm. These same qualities are also characteristic of Pe.

Stern−volmer-Like Fluorescence Quenching Using Electrochemically Generated [BP-H]$^-$ and Its Unusual Dependence on Hydroxide Concentration. Having identified the most likely structure of [**BP-H**]$^-$, we return to explorations of photoluminescence as a function of the added substrate, recalling our earlier observation that the emission intensity is diminished in the presence of benzene. As was noted, those preliminary studies involved chromophores generated nonquantitatively under photolysis conditions in the presence of excess TMAOH. Here, we rely on the bulk electrolysis procedures developed above to produce [**BP-H**]$^-$ more cleanly, without inclusion of hydroxide, for systematic interrogation. **BPDE** was electrolyzed in a THF/tAmOH/MeOH mixed solvent system using 0.1 M $TBAPF_6$ as the supporting electrolyte to form [**BP-H**]$^-$; subsequently, a small amount of this solution was diluted with 2:1 THF/MeOH to prepare samples. Substrate was then added in varying amounts (i.e., [Q]) and the integrated emission intensity (*F*) relative to the case where [Q] = 0 (i.e., F_0) is used to obtain the Stern−Volmer quenching constant K_{SV} (eq S1).

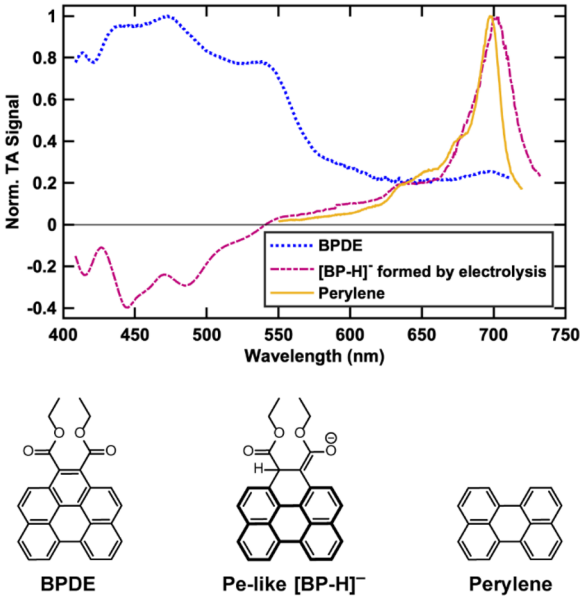

Figure 6. Comparison of TA spectra obtained for **BPDE** with that of the [**BP-H**]$^-$ species formed by bulk electrolysis. All of the spectra were collected by exciting the sample at 398 nm and taking a spectral slice 100 ps after the pump excitation. Since the [**BP-H**]$^-$ species is electrochemically generated, there is a small amount of **BPDE** present in the solution. However, given the stark difference in their spectral profiles, we estimate the contribution from **BPDE** to be very minimal. The excited-state absorption (ESA) of pure perylene (Pe) in EtOH is plotted for comparison. The Pe-like polyaromatic core of [**BP-H**]$^-$ is highlighted for clarification.

We first considered the Pe-like emission intensity of [**BP-H**]$^-$ as a function of the benzene concentration in the absence of hydroxide. In these experiments, emission intensity quenching is minimal (see black circles in Figure 7A in Stern−Volmer plots). Additionally, we do not observe a meaningful decrease in the emission intensity with the addition of more easily reducible substrate 4-fluorobenzonitrile (Figure S31B). This led us to consider the role of hydroxide since it is present in excess when [**BP-H**]$^-$ is produced under photolysis conditions. Benzene was chosen as the quencher for these studies, as it is considered to be very inert and difficult to reduce. Interestingly, the Stern−Volmer constant (K_{SV}) dramatically increases from 0.06 to 0.37 M^{-1} (a 517% enhancement) as the concentration of TMAOH is increased from 0 to 185 mM (Figure 7A). It is noted that with additional increases in concentration from here, the changes to K_{SV} appear muted. At 320 mM added TMAOH, K_{SV} = 0.42 M^{-1}, representing only a 13% increase. The potential relevance of the tetramethylammonium cation, as opposed to the

https://doi.org/10.1021/acscatal.3c05386
ACS Catal. 2024, 14, 2252−2263

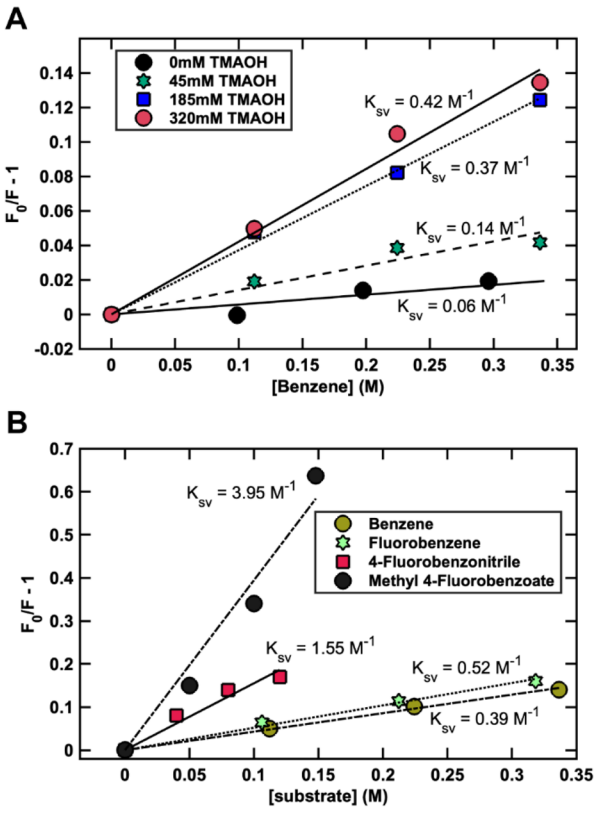

Figure 7. (A) Effect of TMAOH concentration in determining the Stern–Volmer rate constant with benzene as the quencher. (B) Stern–Volmer quenching rates for four different substrates with varying reduction potentials in the presence of 300 mM TMAOH. Both experiments were done with the electrochemically generated $[\mathbf{BP\text{-}H}]^-$ species in a 2:1 THF/MeOH solvent system.

hydroxide, is ruled out in studies using added TMACl, where minimal quenching is observed (see Figure S34 for details).

Having identified the relevance of OH^-, we next considered emission quenching with different substrates, keeping the concentration of TMAOH constant at 300 mM. As shown in Figure 7B, the K_{SV} varies substantially. The smallest value of 0.39 M^{-1} (consistent with Figure 7A) is achieved for benzene, and this increases to 0.52 M^{-1} for fluorobenzene, to 1.55 M^{-1} for 4-fluorobenzonitrile, and to 3.95 M^{-1} for methyl 4-fluorobenzoate. This quenching constant increase correlates with reduction potential: the more easily reduced substrates 4-fluorobenzonitrile (E_{red} = −2.38 V vs SCE[34]) and methyl 4-fluorobenzoate (E_{red} = −2.28 V vs SCE[35]) quench the $[\mathbf{BP\text{-}H}]^-$ emission more efficiently, while the less easily reduced substrates fluorobenzene (E_{red} = −2.97 V vs SCE[36]) and ultimately benzene (E_{red} = −3.48 V vs SCE[37]) are successively less efficient. This correlation with substrate reduction potential is evidence that the mode of quenching is electron transfer initiated by photoexcited $[\mathbf{BP\text{-}H}]^-$, in line with our expectations given the final Birch reduction and dehalogenation products for this model catalyst.

Electron Transfer from Photoexcited $[\mathbf{BP\text{-}H}]^-$ to Inert Arenes Requires a Proton Coordinate. While the quenching efficiency correlates with the reduction potential, the functional relationship is not yet identified. There are several complications in elucidating this relationship. For example, with benzene the reaction product from quenching is expected to be the benzene radical anion, whereas for the fluorinated substrates oxidative quenching of photoexcited $[\mathbf{BP\text{-}H}]^-$ is anticipated to then couple with bond dissociation, leading to an aryl radical and fluoride. The reorganization energy associated with either dissociative electron transfer for aryl fluorides or loss of aromaticity for substrates such as benzene is expected to be large, with significant impacts on the rate constant for quenching. However, the details will be case-specific, making comparisons difficult. Interestingly, throughout Stern–Volmer studies used to quantify the quenching process, we see no evidence for significant lifetime variation (Figure S35) as a function of quencher concentration among any of the tested substrates, which span 1.2 eV of driving force for photoinduced ET. These experiments indicate that quenching is induced by a preassociation between the closed-shell species $[\mathbf{BP\text{-}H}]^-$ and the substrate. Such preassociation controlled by binding equilibria would complicate the identification of the functional form for K_{SV}'s driving force dependence.

The balance of observations uncovers an unusual confluence of factors that enable $[\mathbf{BP\text{-}H}]^-$—or related species in this catalyst class—to act as excited-state super-reductants. Due to the outcome of Birch chemistry, one such case being benzene to cyclohexadiene, there is an obvious draw to invoke a $2e^-/1H^+$ reduction of preassociated arenes directly from photoexcited $[\mathbf{BP\text{-}H}]^-$. However, photoinduced single electron transfer (SET) reactivity is sufficient to explain the initial steps in Birch chemistry and, equally as important, also within arene dehalogenation reactivity where SET is expected. Furthermore, the method of the reduction from the $[\mathbf{BP\text{-}H}]^{-*}$ to the substrate does not address the observed reliance on the presence of base (OH^-). We posit that proton-coupled electron transfer (PCET) or related proton transfer (PT)/electron transfer (ET) is an operative pathway (PT/ET). Namely, the relatively long-lived perylene-like singlet excited state $[\mathbf{BP\text{-}H}]^{-*}$ engages in SET to the arene substrate, but this is accompanied by proton transfer to hydroxide. The end result is the formation of an arene radical anion (or an aryl radical plus a halide in the case of dehalogenation) and water.

While we do not yet have direct evidence for the order of PT and ET events in this system, the electrochemical evidence suggests that proton motions are a key ingredient needed to trigger reduction events, either through PT/ET or through PCET. First, it is noted that for $[\mathbf{BP\text{-}H}]^-$ no emission peak shifts are observed in the presence of base. In other words, the Pe-like chromophore stores 2.76 eV of energy during its 7 ns lifetime (this corresponds to E_{00} taken as the average of the 0–0 peaks in the absorption and emission measurements; see Figure 4D). In the absence of base, the oxidation of $[\mathbf{BP\text{-}H}]^-$ occurs at ca. −1.0 V vs Fc^+/Fc. Combining these photophysical and electrochemical data, the singlet excited state of $[\mathbf{BP\text{-}H}]^-$ can act as a reductant with −3.76 V of potential ($E_{ox} - E_{00}$) vs Fc^+/Fc. This is potent, approximately 660 meV higher in energy than the recently reported napthalene monoimide-derived closed-shell photoreductant $[NMI(H)]^-$ (−3.1 V vs Fc^+/Fc), but still likely insufficient for SET to substrates such as benzene ($E_{1/2}$ = −3.88 V vs Fc^+/Fc). At the other extreme, full deprotonation of $[\mathbf{BP\text{-}H}]^-$ would produce $\mathbf{BPDE}^{2-}$, a species whose one-electron oxidation occurs at −2.61 V vs Fc^+/Fc such that an excited state storing ∼1.75 eV (estimated from the prominent 710 nm absorbance peak; see Figure 4C) could, in principle, function as a reductant with a remarkable −4.36 V of potential vs Fc^+/Fc. In practice, we do not imagine full deprotonation as the 710 nm absorption

https://doi.org/10.1021/acscatal.3c05386
ACS Catal. 2024, 14, 2252−2263

Scheme 1. Proposed Catalytic Cycle for BPDE-Driven Reductive Transformations Involving Proton-Coupled Electron Transfer (PCET)[a]

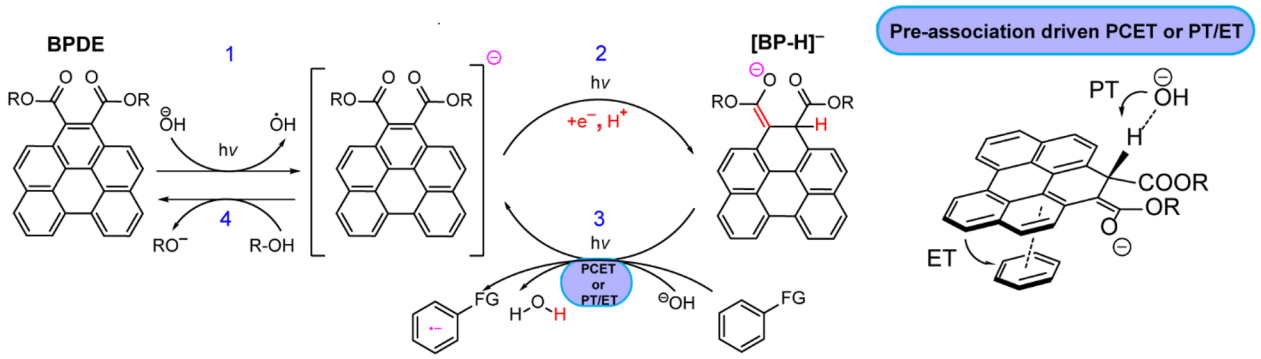

[a](1) Photoinduced electron transfer from hydroxide, acting as the sacrificial reductant, to **BPDE** to form a radical anion, **BPDE**$^{\bullet-}$.[39] (2) An effective e$^-$, H$^+$ reduction of **BPDE**$^{\bullet-}$: (a) a direct hydrogen atom transfer (HAT) from THF to **BPDE**$^{\bullet-}$* or (b) hydroxide oxidation by **BPDE**$^{\bullet-}$* followed by a proton transfer from alcoholic solvent. [**BP-H**]$^-$ is generated in both cases. (3) Photoinduced electron transfer from [**BP-H**]$^-$* to the substrate, along with proton transfer to hydroxide to form water. Pre-association is necessary for the connected PT and ET events to take place. (4) Oxidation of **BPDE**$^{\bullet-}$ to neutral **BPDE**.

feature characteristic of **BPDE**$^{2-}$ is not observed even in the presence of excess TMAOH. Rather, we envision [**BP-H**]$^-$ as a weak acid where fluctuations on a proton transfer coordinate trigger electron transfer events for those [**BP-H**]$^-$ species coordinated with a substrate (Scheme 1). The relevance of base in a related context has recently been described by Bortolato et al. for dihydroacridine photocatalysts with excited-state oxidation potentials up to −3.21 V vs Fc^+/Fc.[38] This notion of a weak acid in the presence of a strong base is consistent with the observations described above involving a rapid increase in K_{SV} with added OH$^-$ followed by a more muted response with additional OH$^-$, reflecting reactivity in what would be a buffer region for the system. This overall model, where both substrate binding and acid/base interactions are governed by equilibria, is consistent with the lack of observation of dynamic quenching. The probability of simultaneous collisions among three species ([**BP-H**]$^-$, substrate, and OH$^-$) leading to a favorable geometry, necessary for the needed PT and ET motions, is low, and as a result the fluorescence lifetime of the [**BP-H**]$^-$ complex remains unaffected even while static quenching can be observed. We expect the binding interaction to be weak with only a minor population of [**BP-H**]$^-$ being preassociated. This limits our ability to detect a change in the UV−vis spectrum as a result of the substrate binding event. We also speculate that reorganization energy following SET from [**BP-H**]$^-$ is substantial, perhaps being coupled to proton loss and subsequent delocalization of the radical in the product **BPDE**$^{\bullet-}$. This could then slow down SET in collisional settings, with any emission quenching requiring the interconnected PT and ET events and with them the need for substrate binding equilibria and an environment inclusive of proton-accepting basic sites.

CONCLUSION

In this work, we first acknowledged the standing limitations of the photo-Birch system, which includes multiple catalyst loadings and long reaction times. The key findings are that the benzo[*ghi*]perylene monoimide (BPI) photocatalyst family is subject to ring opening under the photo-Birch reaction conditions. Additionally, **BPI-P**$^{\bullet-}$ demonstrated a short excited-state lifetime (10 ps), and a doublet open-shell species is an unlikely photoactive intermediate in this system. Discovery of the ring-opening led us to prepare and study a diester-functionalized benzo[*ghi*]perylene model system, **BPDE**, which has proved useful in spectroscopy, electrochemistry, and computational studies, to understand how this new photocatalyst family can achieve challenging reduction chemistries. There are two main interrelated findings within this work. The first centers around the formation and function of an active perylene-like [**BP-H**]$^-$ that is generated as a 2e$^-$/1H$^+$ product from **BPDE**. The second centers around how the chromophore [**BP-H**]$^-$ is able to achieve remarkable potency as an excited state reductant.

During catalysis, we have found a reliance on the presence of OH$^-$ in excess, and the studies herein indicate that it functions in dual roles. The first role is described in this paragraph, and the second role is described in the paragraph that follows. Hydroxide first serves as an electron donor, acting to produce **BPDE**$^{\bullet-}$ from photoexcited **BPDE*** (Scheme 1, 1).[40,41] Following a second photon absorption event, **BPDE**$^{\bullet-}$* could (a) abstract a hydrogen atom from THF[42] to form [**BP-H**]$^-$ or (b) undergo a second oxidization of hydroxide[43] to transiently produce **BPDE**$^{2-}$, which in an alcoholic environment would abstract a proton to also form [**BP-H**]$^-$ (Scheme 1, 2). [**BP-H**]$^-$ exhibits privileged properties relative to its precursors. For example, its absorption spectrum is red-shifted relative to that of **BPDE**, and its S_1 excited-state lifetime is lengthened by almost three orders of magnitude relative to **BPI-P**$^{\bullet-}$* (7 ns compared to ∼10 ps, respectively). The emergent properties of [**BP-H**]$^-$ are made possible by the structure of starting **BPDE**. For example, the π-system supports the first reduction generating the radical anion, while the ester functionalities can accommodate additional reduction through enol tautomerization. Most importantly, rehybridization of a benzo-ring carbon atom from sp^2 to sp^3 results in an effective indirect hydride addition (2e$^-$/1H$^+$), forming stable closed-shell molecule [**BP-H**]$^-$ that exhibits a perylene chromophore core. Rehybridization would presumably be hindered by strain in systems with intact ring structures such as benzo[*ghi*]perylene imides or anhydrides.

As an electron-rich chromophore, [**BP-H**]$^-$ is poised to function as an excited state reductant. Its ground state oxidation, which we observe as a byproduct in the electro-

https://doi.org/10.1021/acscatal.3c05386
ACS Catal. 2024, 14, 2252−2263

chemical experiments, is relatively facile. This, coupled with a 7 ns storage of 2.76 eV of S_1 energy typical for a perylene core, means that [**BP-H**]$^{-}$* is potent with −3.76 V (vs Fc^{+}/Fc) reducing power. However, this is still thermodynamically insufficient to reduce benzene and suggests the second role played by OH^{-}, which now acts as a base rather than a reductant. We envision that those fluctuations on a proton-transfer coordinate—involving the same H atom added during the protonation of **BPDE**$^{2-}$—enervates the excited chromophore for challenging reduction events. Once the electron tunnels, the proton can fully transfer to hydroxide generating water and **BPDE**$^{\bullet-}$ (Scheme 1, 3), thus insulating against nonproductive back electron transfer events. Finally, **BPDE**$^{\bullet-}$ can oxidize back to **BPDE** through reduction of alcohols, present in excess in the reaction mixture (Scheme 1, 4) or reenter the catalytic cycle by reforming [**BP-H**]$^{-}$ following another photoinduced reduction and proton addition.

To our knowledge, no other excited state species, to date, has been reported to be quenched by a substrate as inert as benzene, discovering a new mode to perform challenging reductions without the need of solvated electrons, as previously proposed in the BPI system.[14] To this end, [**BP-H**]$^{-}$ should find utility in designing highly potent PCs to harvest multiphoton energies. The fact that the overall photo-Birch yield by the **BPDE** system is reduced compared to that of the original catalyst (**BPI-P**) could be related to a few things: a difference in the reorganization energy associated with ET to the substrate, a higher rate of back electron transfer from the reduced substrate, or weaker binding between the substrate and the non-core-extended [**BP-H**]$^{-}$. Although **BPDE** is not a high performing photocatalyst in its own right, it provides mechanistic clarity. The uncovered mode of operation—electron transfer to inert substrates originating from a photoexcited $2e^{-}/1H^{+}$ species that involves a proton transfer coordinate—can be readily transferred to other diester-functionalized polyaromatic hydrocarbon motifs. We envision these future diester-based PCs to demonstrate improved reactivity and overcome the limitations of the original BPI-based photo-Birch work with lower PC loadings and faster reaction times toward a new and improved synthetic methodology.

■ ASSOCIATED CONTENT

Supporting Information

The Supporting Information is available free of charge at https://pubs.acs.org/doi/10.1021/acscatal.3c05386.

Reaction details about catalyst synthesis, NMR data, electrochemical data, photophysical data, and computational details (PDF)

■ AUTHOR INFORMATION

Corresponding Authors

Niels H. Damrauer − *Department of Chemistry, University of Colorado Boulder, Boulder, Colorado 80309, United States; Renewable and Sustainable Energy Institute, University of Colorado Boulder, Boulder, Colorado 80309, United States;* orcid.org/0000-0001-8337-9375; Email: niels.damrauer@colorado.edu

Garret M. Miyake − *Department of Chemistry, Colorado State University, Fort Collins, Colorado 80523, United States;* orcid.org/0000-0003-2451-7090; Email: garret.miyake@colostate.edu

Authors

Arindam Sau − *Department of Chemistry, University of Colorado Boulder, Boulder, Colorado 80309, United States*

Nicholas F. Pompetti − *Department of Chemistry, University of Colorado Boulder, Boulder, Colorado 80309, United States*

Alexander R. Green − *Department of Chemistry, Colorado State University, Fort Collins, Colorado 80523, United States*

Mihai V. Popescu − *Department of Chemistry, Colorado State University, Fort Collins, Colorado 80523, United States*

Robert S. Paton − *Department of Chemistry, Colorado State University, Fort Collins, Colorado 80523, United States;* orcid.org/0000-0002-0104-4166

Complete contact information is available at: https://pubs.acs.org/10.1021/acscatal.3c05386

Author Contributions

$^{\nabla}$A.S., N.F.P., and A.R.G. all contributed to this work equally.

Notes

The authors declare no competing financial interest.

■ ACKNOWLEDGMENTS

We would like to acknowledge Dr. Max Kudisch and Dr. Yisreal Lamb for their excellent mentorship and positivity in helping us at the beginning of these mechanistic studies. Thank you to the ARC at CSU with research resource ID SCR_021758. This work was supported by the National Science Foundation (NSF) under award no. 2016557, the National Institutes of Health under award no. R35GM144356, Colorado State University, and the University of Colorado Boulder. The content is solely the responsibility of the authors and does not necessarily represent the official views of the NSF.

■ REFERENCES

(1) Romero, N. A.; Nicewicz, D. A. Organic Photoredox Catalysis. *Chem. Rev.* **2016**, *116* (17), 10075−10166.

(2) Corbin, D. A.; Swisher, N. A.; Miyake, G. M. Fundamentals of Photochemical Redox Reactions. *Organic Redox Chemistry: Chemical, Photochemical and Electrochemical Syntheses* **2021**, 45−102.

(3) Chan, A. Y.; Perry, I. B.; Bissonnette, N. B.; Buksh, B. F.; Edwards, G. A.; Frye, L. I.; Garry, O. L.; Lavagnino, M. N.; Li, B. X.; Liang, Y.; et al. Metallaphotoredox: the merger of photoredox and transition metal catalysis. *Chem. Rev.* **2022**, *122* (2), 1485−1542.

(4) McAtee, R. C.; McClain, E. J.; Stephenson, C. R. Illuminating photoredox catalysis. *Trends Chem.* **2019**, *1* (1), 111−125.

(5) Bell, J. D.; Murphy, J. A. Recent advances in visible light-activated radical coupling reactions triggered by (i) ruthenium,(ii) iridium and (iii) organic photoredox agents. *Chem. Soc. Rev.* **2021**, *50* (17), 9540−9685.

(6) Skubi, K. L.; Blum, T. R.; Yoon, T. P. Dual catalysis strategies in photochemical synthesis. *Chem. Rev.* **2016**, *116* (17), 10035−10074.

(7) Ghosh, I.; Ghosh, T.; Bardagi, J. I.; König, B. Reduction of aryl halides by consecutive visible light-induced electron transfer processes. *Science* **2014**, *346* (6210), 725−728.

(8) Glaser, F.; Kerzig, C.; Wenger, O. S. Multi-Photon Excitation in Photoredox Catalysis: Concepts, Applications, Methods. *Angew. Chem., Int. Ed. Engl.* **2020**, *59* (26), 10266−10284.

(9) MacKenzie, I. A.; Wang, L.; Onuska, N. P. R.; Williams, O. F.; Begam, K.; Moran, A. M.; Dunietz, B. D.; Nicewicz, D. A. Discovery and characterization of an acridine radical photoreductant. *Nature* **2020**, *580* (7801), 76−80.

(10) Zeman, C. J. t.; Kim, S.; Zhang, F.; Schanze, K. S. Direct Observation of the Reduction of Aryl Halides by a Photoexcited

Perylene Diimide Radical Anion. *J. Am. Chem. Soc.* **2020**, *142* (5), 2204−2207.
(11) Cowper, N. G. W.; Chernowsky, C. P.; Williams, O. P.; Wickens, Z. K. Potent Reductants via Electron-Primed Photoredox Catalysis: Unlocking Aryl Chlorides for Radical Coupling. *J. Am. Chem. Soc.* **2020**, *142* (5), 2093−2099.
(12) Kim, H.; Kim, H.; Lambert, T. H.; Lin, S. Reductive Electrophotocatalysis: Merging Electricity and Light To Achieve Extreme Reduction Potentials. *J. Am. Chem. Soc.* **2020**, *142* (5), 2087−2092.
(13) Glaser, F.; Wenger, O. S. Red Light-Based Dual Photoredox Strategy Resembling the Z-Scheme of Natural Photosynthesis. *JACS Au* **2022**, *2* (6), 1488−1503.
(14) Cole, J. P.; Chen, D. F.; Kudisch, M.; Pearson, R. M.; Lim, C. H.; Miyake, G. M. Organocatalyzed Birch Reduction Driven by Visible Light. *J. Am. Chem. Soc.* **2020**, *142* (31), 13573−13581.
(15) Chatterjee, A.; Konig, B. Birch-Type Photoreduction of Arenes and Heteroarenes by Sensitized Electron Transfer. *Angew. Chem., Int. Ed. Engl.* **2019**, *58* (40), 14289−14294.
(16) Goez, M.; Hussein, B. H. M. Photoionization of xanthone via its triplet state or via its radical anion. *Phys. Chem. Chem. Phys.* **2004**, *6* (24), 5490−5497.
(17) Fujita, M.; Ishida, A.; Majima, T.; Takamuku, S. Lifetimes of Radical Anions of Dicyanoanthracene, Phenazine, and Anthraquinone in the Excited State from the Selective Electron-Transfer Quenching. *J. Phys. Chem.* **1996**, *100* (13), 5382−5387.
(18) Gosztola, D.; Niemczyk, M. P.; Svec, W.; Lukas, A. S.; Wasielewski, M. R. Excited Doublet States of Electrochemically Generated Aromatic Imide and Diimide Radical Anions. *J. Phys. Chem. A* **2000**, *104* (28), 6545−6551.
(19) Fujitsuka, M.; Majima, T. Reaction dynamics of excited radical ions revealed by femtosecond laser flash photolysis. *J. Photochem. Photobiol. C* **2018**, *35*, 25−37.
(20) Rieth, A. J.; Gonzalez, M. I.; Kudisch, B.; Nava, M.; Nocera, D. G. How Radical Are "Radical" Photocatalysts? A Closed-Shell Meisenheimer Complex Is Identified as a Super-Reducing Photoreagent. *J. Am. Chem. Soc.* **2021**, *143* (35), 14352−14359.
(21) Li, H.; Wenger, O. S. Photophysics of Perylene Diimide Dianions and Their Application in Photoredox Catalysis. *Angew. Chem., Int. Ed. Engl.* **2022**, *61* (5), No. e202110491.
(22) Emmett, P.; Skau, N. The catalytic hydrogenation of benzene over metal catalysts. *J. Am. Chem. Soc.* **1943**, *65* (6), 1029−1035.
(23) Birch, A. Reduction by dissolving metals. Part I. *J. Chem. Soc.* **1944**, 430−436.
(24) Kwon, Y.; Lee, J.; Noh, Y.; Kim, D.; Lee, Y.; Yu, C.; Roldao, J. C.; Feng, S.; Gierschner, J.; Wannemacher, R.; et al. Formation and degradation of strongly reducing cyanoarene-based radical anions towards efficient radical anion-mediated photoredox catalysis. *Nat. Commun.* **2023**, *14*, 92.
(25) Marchini, M.; Gualandi, A.; Mengozzi, L.; Franchi, P.; Lucarini, M.; Cozzi, P. G.; Balzani, V.; Ceroni, P. Mechanistic insights into two-photon-driven photocatalysis in organic synthesis. *Phys. Chem. Chem. Phys.* **2018**, *20* (12), 8071−8076.
(26) Han, X.; Li, H.-M.; Xu, C.; Xiao, Z.-Q.; Wang, Z.-Q.; Fu, W.-J.; Hao, X.-Q.; Song, M.-P. Water-soluble palladacycles containing hydroxymethyl groups: synthesis, crystal structures and use as catalysts for amination and Suzuki coupling of reactions. *Transition Met. Chem.* **2016**, *41* (4), 403−411.
(27) Manning, S. J.; Bogen, W.; Kelly, L. A. Synthesis, characterization, and photophysical study of fluorescent N-substituted benzo[ghi]perylene "swallow tail" monoimides. *J. Org. Chem.* **2011**, *76* (15), 6007−13.
(28) Bowden, K.; Hiscocks, S. P.; Perjéssy, A. Ring-chain tautomerism. Part 9.1 2-Acylbenzamides, 8-acyl-1-naphthamides and 5-acyl-4-phenanthramides. *J. Chem. Soc., Perkin Trans. 2* **1998**, 291−296.
(29) Clar, E.; Ironside, C. T.; Zander, M. Annellation effects in the perylene and coronene series. *Tetrahedron* **1966**, *22* (10), 3527−3533.
(30) Guha, S.; Goodson, F. S.; Corson, L. J.; Saha, S. Boundaries of anion/naphthalenediimide interactions: from anion-pi interactions to anion-induced charge-transfer and electron-transfer phenomena. *J. Am. Chem. Soc.* **2012**, *134* (33), 13679−91.
(31) Saha, S. Anion-Induced Electron Transfer. *Acc. Chem. Res.* **2018**, *51* (9), 2225−2236.
(32) Shida, T.; Iwata, S. Electronic spectra of ion radicals and their molecular orbital interpretation. III. Aromatic hydrocarbons. *J. Am. Chem. Soc.* **1973**, *95* (11), 3473−3483.
(33) Thielen, D.; Anderson, L. Electrochemical irreducibility of the cyclooctatetraene radical anion. *J. Am. Chem. Soc.* **1972**, *94* (7), 2521−2523.
(34) Muthukrishnan, A.; Sangaranarayanan, M. V. Electrochemical reduction of carbon-fluorine bond in 4-fluorobenzonitrile - Mechanistic analysis employing Marcus-Hush quadratic activation-driving force relation. *Chem. Phys. Lett.* **2007**, *446* (4), 297−303.
(35) Muthukrishnan, A.; Sangaranarayanan, M. V. Analysis of C-F bond cleavages in methylfluorobenzoates—Fragmentation and dimerization of anion radicals using convolution potential sweep voltammetry. *Electrochim. Acta* **2010**, *55* (5), 1664−1669.
(36) Andrieux, C. P.; Blocman, C.; Savéant, J. M. Characterization of electrochemical reactions hidden in the background discharge the redox catalyzed reduction of fluorobenzene. *J. Electroanal. Chem. Interfacial Electrochem.* **1979**, *105* (2), 413−417.
(37) Mortensen, J.; Heinze, J. The Electrochemical Reduction of Benzene—First Direct Determination of the Reduction Potential. *Angew. Chem., Int. Ed. Engl.* **1984**, *23* (1), 84−85.
(38) Bortolato, T.; Simionato, G.; Vayer, M.; Rosso, C.; Paoloni, L.; Benetti, E. M.; Sartorel, A.; Leboeuf, D.; Dell'Amico, L. The Rational Design of Reducing Organophotoredox Catalysts Unlocks Proton-Coupled Electron-Transfer and Atom Transfer Radical Polymerization Mechanisms. *J. Am. Chem. Soc.* **2023**, *145* (3), 1835−1846.
(39) Another slightly more complex mechanism is also possible that we cannot rule out at this time. As argued in the text and reiterated in this caption regarding step 2 of the mechanism, HAT from THF could play a role producing [**BP-H**]$^-$. It is also possible that HAT plays a role in step 1. Therein, HAT from THF to **BPDE*** would produce a transient product [**BPDE-H**]$^\bullet$ (and a THF radical). With hydroxide present, [**BPDE-H**]$^\bullet$ could then deprotonate, leading to **BPDE**$^{\bullet-}$ plus water.
(40) Based on the $E_{0,0}$ value of 2.86 eV (i.e., the amount of energy stored in the relaxed **BPDE** S_1 state as determined from the intersection between the absorption and emission spectra), along with **BPDE**'s first reduction potential (−2.22 V vs Fc^+/Fc), we estimate the redox potential available for hydroxide oxidation to be 0.64 V vs Fc^+/Fc by **BPDE*** in its S_1 excited state. While we were unable to find an oxidation potential of OH^- in a THF/MeOH mixture, our solvent system, the reported value of 0.28 V vs Fc^+/Fc in MeCN (cf. 41) would suggest that **BPDE*** is indeed capable of oxidizing OH^-. We do acknowledge that this number is not a true resentative of the OH^- oxidation potential in our system due to presence of protic MeOH in the solvent mixture. However, we feel that it is indeed reasonable to expect that the oxidation potential would still be within a range accessible by **BPDE***.
(41) Sawyer, D. T.; Roberts, J. L., Jr Hydroxide ion: an effective one-electron reducing agent? *Acc. Chem. Res.* **1988**, *21* (12), 469−476.
(42) Jing, L.; Nash, J. J.; Kenttämaa, H. I. Correlation of hydrogen-atom abstraction reaction efficiencies for aryl radicals with their vertical electron affinities and the vertical ionization energies of the hydrogen-atom donors. *J. Am. Chem. Soc.* **2008**, *130* (52), 17697−17709.
(43) In terms of the second hydroxide oxidation event, it is noted that it is challenging to estimate $E_{0,0}$ for the lowest excited doublet state of **BPDE**$^{\bullet-}$ because that species is nonemissive. Since we are able to detect weak absorption of **BPDE**$^{\bullet-}$ to the red at ∼1000 nm, it can be argued that its D_1 state stores approximately ∼1.2 eV of energy. With this number and given that the **BPDE**$^{\bullet-}$ + e^- ⇌ **BPDE**$^{2-}$ (−2.61 V vs Fc^+/Fc) couple takes place only 390 meV higher than the first reduction **BPDE** + e^- ⇌ **BPDE**$^{\bullet-}$ (−2.22 V vs

https://doi.org/10.1021/acscatal.3c05386
ACS Catal. 2024, 14, 2252−2263

Fc^+/Fc; see Figure 4a in the main text), the potential for oxidation of OH^- by **BPDE**$^{\bullet-}$* is estimated to be 0.85 V vs Fc^+/Fc. This represents an excited state potential with a driving force greater than what was estimated in the first case discussed above involving **BPDE***.

https://doi.org/10.1021/acscatal.3c05386
ACS Catal. 2024, 14, 2252−2263